Properties of High-Impact Polystyrene/Organoclay Nanocomposites Synthesized via *In Situ* Polymerization

Sung Jun Hwang,[1] Yong Lak Joo,[2,3] Seong Jae Lee[1]

[1]*Department of Polymer Engineering, University of Suwon, Gyeonggi, Korea 445-743*
[2]*School of Chemical and Biomolecular Engineering, Cornell University, Ithaca, NY 14853*
[3]*Department of Chemical and Biological Engineering, Korea University, Seoul, Korea 136-701*

Received 10 June 2007; accepted 7 April 2008
DOI 10.1002/app.28546
Published online 17 July 2008 in Wiley InterScience (www.interscience.wiley.com).

ABSTRACT: High-impact polystyrene (HIPS)/organically modified montmorillonite (organoclay) nanocomposites were synthesized via *in situ* polymerization. The effects of the organoclay on the morphology and material properties of HIPS/organoclay nanocomposites were investigated. X-ray diffraction and transmission electron microscopy experiments revealed that intercalation of polymer chains into silicate layers was achieved, and the addition of nanoclay led to an increase in the size of the rubber domain in the composites. In comparison with neat HIPS, the HIPS/organoclay nanocomposites exhibited improved thermal stability as well as an increase in both the complex viscosity and storage modulus. The presence of intercalated organoclay drastically enhanced the gas-barrier properties because of the increase in the tortuosity of the diffusive path for a penetrating gas molecule. Some mechanical properties, including the tensile modulus, were superior to those of conventional HIPS. Finally, the preparation of the nanocomposites with a minimal loss of impact properties was proposed through changes in the synthetic procedure. © 2008 Wiley Periodicals, Inc. J Appl Polym Sci 110: 1441–1450, 2008

Key words: nanocomposites; organoclay; polystyrene; synthesis

INTRODUCTION

The inclusion of organically modified clay in a polymer matrix has been used as an attractive means of improving various material properties, including stiffness, dimensional stability, barrier properties, thermal stability, and flame retardancy.[1–3] During the last decade, many researchers have focused on improving the properties of thermoplastics such as polystyrene (PS) by incorporating organically modified clays into a polymer matrix via *in situ* polymerization,[4–9] but studies on nanocomposites based on rubber-toughened PS are rare to the best of our knowledge.[10] Rubber-toughened PS, also known as high-impact polystyrene (HIPS), offers enhancements of the impact strength and toughness of glassy PS. Its major applications include packaging, containers, appliance parts, house wares, and interior parts in household electronics. Imperative research on HIPS is the development of various high-performance grades, and the introduction of organoclay is a logical route for enhancing the chemical resistance, mechanical strength, and flame retardancy of HIPS.

Montmorillonite is a classic clay mineral for nanocomposite applications; it is about 200 nm long and 1 nm thick. It has a sandwich type of structure called philosilicate with one octahedral Al_2O_3 sheet between two tetrahedral SiO_2 sheets.[1,11–15] Because natural montmorillonite cannot be dispersed in organic solvents on account of its hydrophilic nature, it is necessary to use an ion-exchange reaction with surfactants with alkyl tallow groups to render it organophilic, and this results in an organoclay. When a polymer is unable to intercalate between silicate layers, a phase-separated composite is obtained, the properties of which stay in the same range as that of traditional microcomposites. For preparing polymer/clay nanocomposites with better clay dispersion, four main strategies have been considered, with each component—clay, organic modifier, and polymer—being tuned: exfoliation adsorption, *in situ* intercalative polymerization, melt intercalation, and template synthesis.[12,16,17]

In this study, *in situ* intercalative polymerization was used. HIPS/organoclay nanocomposites with various rubber and organoclay contents were synthesized via *in situ* free-radical polymerization, and the characterization of the synthesized nanocomposites was also carried out. First in this article, the effect of the nanoclay inclusion on the morphology of the nanocomposites, including the dispersion of silicate layers in the polymer matrix, and the effect

Correspondence to: S. J. Lee (sjlee@suwon.ac.kr).
Contract grant sponsor: Korean Science and Engineering Foundation (through the Applied Rheology Center).

of the rubber domain size and its distribution are investigated. Then, the material properties of the HIPS/clay nanocomposites, such as thermal, rheological, gas-barrier, and mechanical properties, are compared to those of neat HIPS. In the development of HIPS/organoclay nanocomposites, the decrease in the impact properties caused by the introduction of rigid clay to rubber-toughened materials is inevitable, and a heuristic way of synthesizing nanocomposites to minimize such a loss in impact properties is proposed.

EXPERIMENTAL

Materials

Styrene monomer was purified by vacuum distillation before use. Polybutadiene (PB), the main rubber component, had a molecular weight of 420,000 g/mol and the following monomer unit concentrations: 36% cis, 55% trans, and 9% vinyl. As an initiator, 2,2-azobisisobutyronitrile was used, and it was purified by recrystallization via a methanol precipitation method and used after vacuum drying. Other solvents such as ethyl benzene (EB), toluene, and methyl ethyl ketone were used without further purification. The organoclays used for the synthesis of the HIPS/clay nanocomposites were commercial organoclays from Southern Clay Products (Gonzales, TX) that were organically modified with quaternary ammonium salts from pristine montmorillonite (sodium montmorillonite): Cloisite 10A (C10A), Cloisite 20A (C20A), and Cloisite 30B (C30B). Information on the organic modifiers and modifier concentrations is summarized in Table I. All the organoclays were vacuum-dried before use. The nanocomposites were prepared through the variation of both the rubber content (0, 3, 5, and 8 wt %) and the organoclay content (0, 1, and 3 wt %).

TABLE I
Information on Organoclay Types Based on Different Modifiers

Organoclay	Abbreviation	Organic modifier	Modifier concentration
Cloisite 10A	C10A	2MBzHT	125 mequiv/100 g
Cloisite 20A	C20A	2M2HT	95 mequiv/100 g
Cloisite 30B	C30B	MT2EtOH	90 mequiv/100 g

2MBzH = dimethyl benzyl hydrogenated tallow ammonium salt; 2M2HT = dimethyl dehydrogenated tallow ammonium salt; MT2EtOH = methyl tallow bis-2-hydroxyethyl ammonium salt.

Synthesis of the HIPS/organoclay nanocomposites

The free-radical polymerization of a styrene solution containing the rubber and organoclay was carried out in the following way. First, the clay was dissolved in styrene for 2–6 h according to the clay content. The dissolving time was established from that time at which a stable dispersion was kept and no precipitation of clay was shown under quiescent conditions. Next, the desired amount of PB was weighed, cut into small pieces, and dissolved in the styrene solution for 12 h. Within this period, a PB concentration as high as 8 wt % was fully soluble in the solution. The initiator was charged at a fixed concentration of 0.1 mol % with respect to styrene into the reactor just before the start of polymerization. The polymerization temperature was kept at 70°C. An inert atmosphere was maintained throughout the polymerization with a nitrogen stream. The agitation speed was maintained at 100 rpm during the prepolymerization stage. The total reaction time, including a 6-h prepolymerization, was 48 h. The prepolymerization time, related to the phase inversion between the PS and PB phases, was established by measurements of the conversion, viscosity, and particle size analysis, as described in a previous study.[18] After polymerization, the sample was cut into thin slices and dried for 4 days at 40°C in a vacuum oven to strip off the unreacted monomer and solvent; the drying conditions were gradually changed from a low vacuum to a high vacuum to prevent gas bubbles, and this could affect the morphology of the synthesized sample. The code PB*x*–C10A*y* was used to identify the samples: *x* and *y* stand for the weight percentages of PB and C10A, respectively. For example, PB5–C10A1 indicates a sample prepared with 5 wt % PB and 1 wt % C10A.

Characterization of the nanocomposites

The spacing between silicate layers was measured with an X-ray diffractometer (D/Max 2C, Rigaku, Tokyo, Japan) equipped with nickel-filtered Cu Kα radiation ($\lambda = 1.542$ Å) as an X-ray source. Bragg's law, $n\lambda = 2d \sin\theta$, was used to calculate the basal spacing (d), that is, the sum of a single silicate layer thickness and the interlayer distance between adjacent layers. The rubber-phase morphology and silicate dispersion were examined with transmission electron microscopy (TEM; JEM-2000EX2, JEOL, Tokyo, Japan). TEM samples were prepared with the OsO_4 staining technique. The acceleration voltage was 100 kV.

The particle size distribution of the rubber phase was analyzed with a particle size analyzer (Mastersizer Micro-P, Malvern, Worcestershire, UK) based on the laser light scattering technique. Small sample pieces of about 1.5 g were dissolved in 50 mL of methyl ethyl ketone for 6 h to isolate the rubber-phase particles from the sample. During the rubber particle size analysis experiments, methyl ethyl ketone was used as the circulating medium. The laser light scattered by the resulting dilute suspension was focused on a light detector and then processed

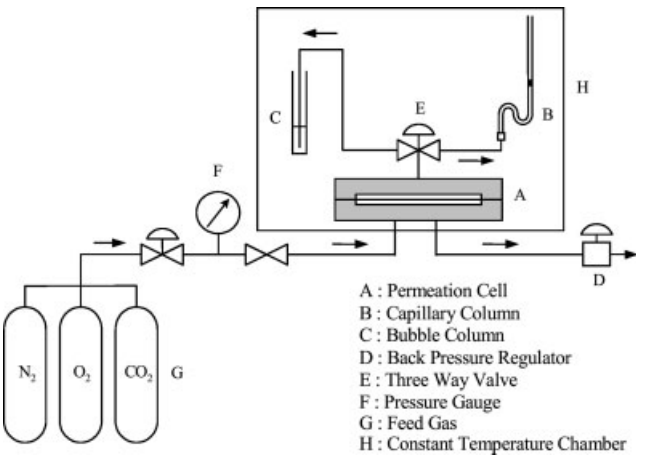

Figure 1 Schematic diagram of the apparatus for the measurement of gas permeability by the variable-volume method.

to provide the particle size distribution of the suspended particles, which ranged from 0.05 to 550 μm.

The thermal properties were determined with a thermogravimetric analyzer (STA 409, Netzsch, Selb, Germany) at a heating rate of 20°C/min to 600°C in a nitrogen environment. The rheological properties were investigated with a rotational rheometer (MCR 300, Paar Physica, Stuttgart, Germany) in the oscillatory shear mode. Samples 1 mm thick with a 25-mm radius were used in a parallel-plate apparatus, and the strain amplitude was imposed to be equal to 3% at a constant temperature of 230°C under a nitrogen flow.

The gas-barrier properties were analyzed for various films of HIPS/organoclay nanocomposite samples. A schematic diagram of the apparatus for the measurement of gas permeability is shown in Figure 1. The permeability of three different gases (nitrogen, oxygen, and carbon dioxide) through the films was measured at 20°C by the variable-volume method.[19] Test films for this measurement were prepared by compression molding, and all prepared films were 5 cm in diameter and approximately 180 ± 20 μm thick. Each film was located inside the permeation cell; a high-pressure gas was applied to the lower part of the cell, and the ambient pressure was maintained in the upper part of the cell. To support the film, two porous metal discs were placed in both parts of the cell, and a paper filter was added to the low-pressure side. The pressure difference between the two parts of the cell was kept at 5 bar, and the volume that permeated through the film was measured against time in a capillary column until a constant gradient was reached.

Mechanical tests were performed with a universal testing machine (LR 50K, Lloyd, Fareham, UK) with dumbbell-type specimens prepared according to ASTM D 638 at a crosshead speed of 50 mm/min. The impact strength was measured with Izod-type specimens prepared according to ASTM D 256.

RESULTS AND DISCUSSION

Rubber morphology and silicate dispersion

The rubber-phase morphology that develops during polymerization can be complex because the organoclay and high-molecular-weight rubber are dissolved in styrene. As the separation of the PS phase and the phase inversion between the PS and PB phases proceed, it is possible that the silicate layers are placed (1) in the PS matrix, (2) in the dispersed PB domain, and (3) at the interface. Figure 2(a) shows X-ray

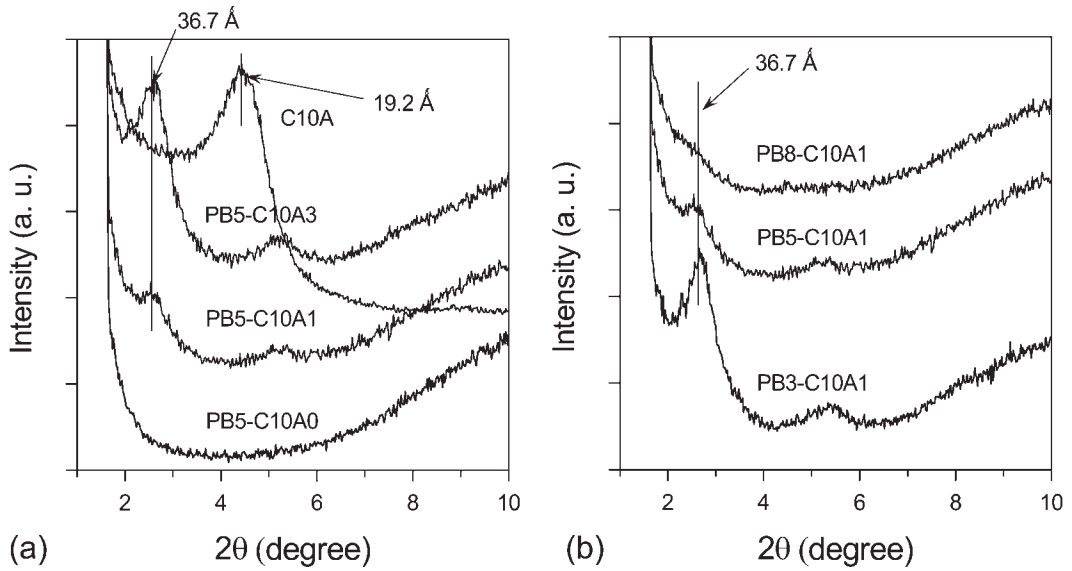

Figure 2 XRD diffractograms of HIPS/organoclay nanocomposites: (a) effect of the clay content and (b) effect of the rubber content.

TABLE II
XRD Peak Values of Organoclays and HIPS/Organoclay Nanocomposites

Organoclay type	d_{001} peak (Å)		
	Organoclay	HIPS/organoclay	Δd (Å)
C10A	19.2	36.7	17.5
C20A	24.2	38.5	14.3
C30B	18.5	32.1	13.6

diffraction (XRD) diffractograms of the organoclay C10A and its nanocomposites with various clay contents at a fixed rubber content of 5 wt %. XRD patterns were recorded through the monitoring of the diffraction angle (2θ) from 1.5 to 10°. The XRD peak of the nanocomposites was confirmed to shift to a lower angle, indicating the intercalation of PS chains into silicate layers. The basal spacing of the HIPS/organoclay nanocomposites with 1 or 3 wt % C10A was 36.7 Å, whereas that of the organoclay was 19.2 Å; these were calculated from the peak position with Bragg's law. The XRD patterns of nanocomposites with various rubber contents at a fixed organoclay content of 1 wt % are shown in Figure 2(b). The peak intensity of the nanoclay weakens because of the scattering effect of the rubber-phase domain as the PB content increases. When styrene monomer penetrates the organoclay interlayer and polymerizes, a substantial increase in the interlayer distance occurs because the organoclay structures contain a benzyl group similar to styrene. As summarized in Table II, the difference in the basal spacings between C10A and its nanocomposite was larger than those for the others, C20A and C30B. These results may imply that the insertion of growing polymer chains during polymerization can be facilitated not only by the organophilicity of organic groups but also by the structural affinity between the monomer used and the organic group of the organoclay. Nanocomposites with C10A that exhibited the largest interlayer distance were used in the following study of the effects of the organoclay on the morphology and material properties of the nanocomposites.

Figure 3 presents TEM micrographs of neat HIPS and HIPS/organoclay nanocomposites, showing the rubber-phase particle size and morphology. It is not

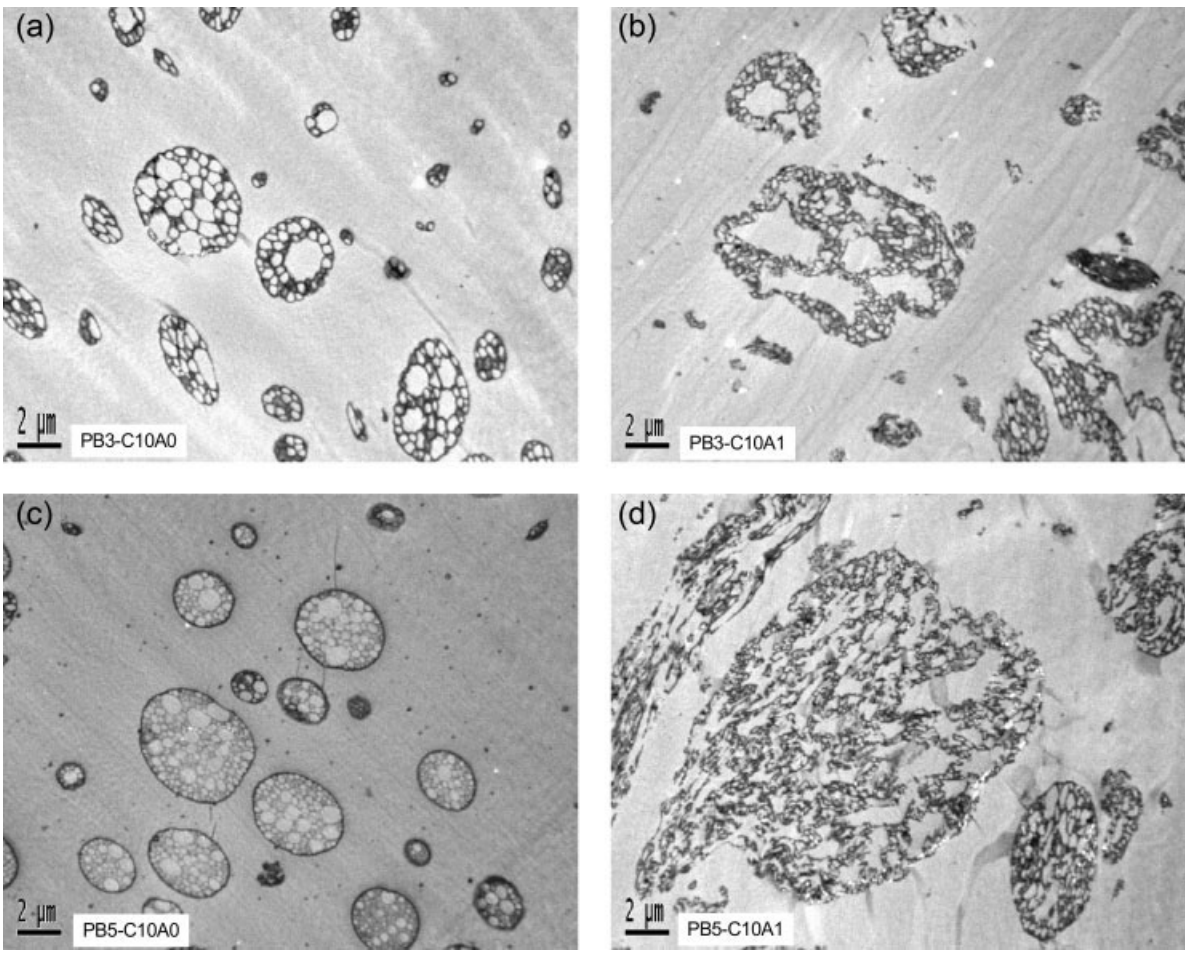

Figure 3 TEM micrographs of HIPS and HIPS/organoclay nanocomposites showing the rubber-phase morphology: (a) HIPS (PB3–C10A0), (b) HIPS/organoclay (PB3–C10A1), (c) HIPS (PB5–C10A0), and (d) HIPS/organoclay (PB5–C10A1).

quite clear that the size of the rubber particles in organoclay-free HIPS increases with increasing rubber content from an evaluation of the morphology shown in Figure 3(a,c). However, the average rubber-phase particle diameter from the laser light scattering experiments in Table III indicates that the size of the rubber particles in HIPS increases with increasing rubber content. Previous studies have also revealed that the size of rubber-phase particles in HIPS increases with increasing rubber content.[20,21] The incorporation of organoclay leads to an increasing effect on the rubber-phase domain size and makes the domain shapes more irregular, as shown in Figure 3(a,b) for 3% PB and in Figure 3(c,d) for 5% PB. The average rubber-phase particle diameters of HIPS and HIPS/organoclay nanocomposites are summarized in Table III. At a given PB content, the HIPS samples without any organoclay show both small particle sizes and narrow size distributions of the rubber domains. It can easily be surmised that the phase inversion from the continuous PB phase to the dispersed PB phase during the course of *in situ* polymerization is impeded by the presence of silicate layers with a high aspect ratio. There might also be a bridging effect due to the existence of silicate layers. As a result, the average rubber-phase particle size and its distribution in the HIPS/organoclay nanocomposites are larger and broader, respectively, than those of their counterparts without clay.

The TEM micrographs of HIPS/organoclay nanocomposites are presented in Figure 4, which shows the degree of dispersion of silicate layers inside the host polymers. Silicate layers are well distributed both in the PS phase and in the PB phase, as shown in Figure 4(a,b), respectively. As shown by the XRD results in Figure 2(a), the nanocomposites exhibit an intercalated structure. Figure 4(b) shows that the silicate layers with long aspect ratios are located within the dispersed rubber domain and at the interface between the rubber and matrix phases. This reveals that the rigid, long, disc-shaped silicate layers can act as obstacles when phase inversion occurs during polymerization, resulting in large rubber-phase particles, as already described in Figure 3 and Table III. In the commercial manufacturing processes of HIPS, the solution polymerization technique of HIPS is also widely used in addition to bulk polymerization. A series of solution runs with EB as a diluent are used to reduce the viscosity increase of reaction

TABLE III
Average Rubber-Phase Particle Diameters of HIPS and HIPS/Organoclay Nanocomposites

Sample code	D_{32} (μm)	$D_{0.5}$ (μm)	D_{43} (μm)
PB3–C10A0	5.08	5.85	6.25
PB3–C10A3	5.20	8.15	9.39
PB5–C10A0	5.76	6.20	6.46
PB5–C10A3	11.54	21.01	26.07
PB8–C10A0	11.03	14.61	18.90
PB8–C10A3	18.18	65.00	79.08

$D_{0.5}$ = cumulative mean diameter; D_{32} = volume surface (or Sauter) mean diameter; D_{43} = volume mean diameter.

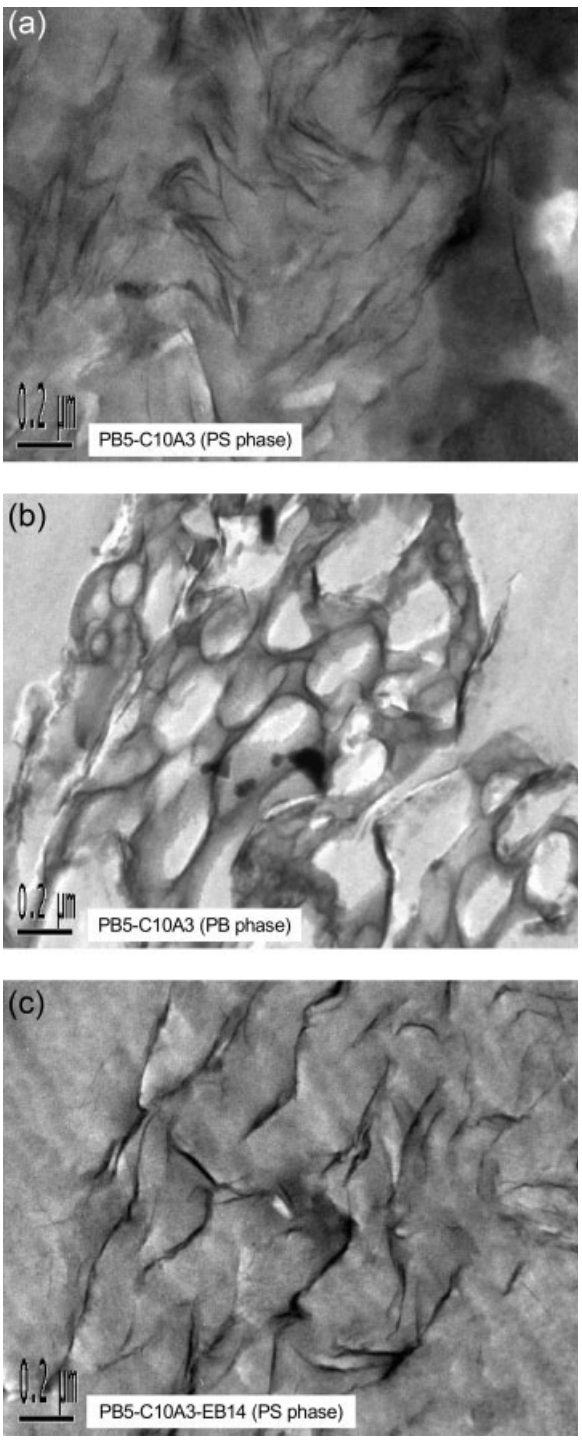

Figure 4 TEM micrographs of HIPS/organoclay nanocomposites showing silicate dispersions: (a) the dispersion in the PS phase (PB5–C10A3), (b) the dispersion in the PB phase (PB5–C10A3), and (c) the dispersion in the PS phase (PB3–C10A3–EB14).

intermediates and to dissipate the reaction heat during polymerization. A detailed description of solution polymerization based on solution runs with EB can be found elsewhere.[22] In the case of the solution run, however, the silicate dispersion is not as good as bulk runs, as shown in Figure 4(c). It seems that clay bundles are randomly dispersed in the polymer matrix, but the silicate layers in a clay bundle exist in a stacked and flocculated structure composed of tens of silicate layers. Accordingly, the material properties of the composite prepared by the solution-run *in situ* polymerization of HIPS/organoclay with EB as a diluent and C10A as a clay were inferior to those of the one prepared by a bulk run (not shown here).

Thermal and rheological properties

The effects of the organoclay on the thermal stability of the nanocomposites can be seen in the thermogravimetric analysis (TGA) thermograms in Figure 5. For the thermal analysis of HIPS/organoclay nanocomposites, specimens of about 10 mg were heated to 600°C at a heating rate of 20°C/min. Evidently, the decomposition temperature of those nanocomposites shifted toward a temperature range higher than that of HIPS without any clay. The decomposition temperature with 50% of the weight remaining increased about 14°C from 446 to 460°C with the addition of 1% organoclay. The effect of the clay on the substantial increase in the degradation temperature can be explained by the silicate layers with high aspect ratios, which could hinder the permeability of volatile degradation matter out of the polymer matrix. Other researchers have also observed that silicate layers act as heat barriers and thus enhance the overall thermal stability of the system. In addition, these silicate layers assist with the formation of char after thermal decomposition.[5,8,9,12,23] However, the sample prepared with 3% organoclay did not show a further improvement in thermal stability. This is in agreement with findings of a previous study, which showed that at very low filler contents, a large increase in the onset of decomposition occurs, and thermal decomposition quickly levels off.[5] From these results, it is suspected that the polymerization rate slowed down because of the higher clay content, and thus the conversion was incomplete at a specified reaction time. A higher weight loss at the initial stage with increasing clay content supports this insight, as shown in Figure 5. The average molecular weights of PS in the HIPS/organoclay nanocomposites were measured by gel permeation chromatography, and the results are summarized in Table IV. The weight-average molecular weight decreased with both the clay content and the rubber content. A reduction in the molecular weight with increasing clay content has been reported for PS/organoclay syntheses and has been attributed to the silicate layers hindering PS chain growth.[8,9] This decrease in the matrix molecular weight at high clay contents also explains our TGA results showing that the thermal stability is not proportional to the clay content. The improvement in the thermal properties may lead to greater performance of HIPS/organoclay nanocomposites at higher temperatures.

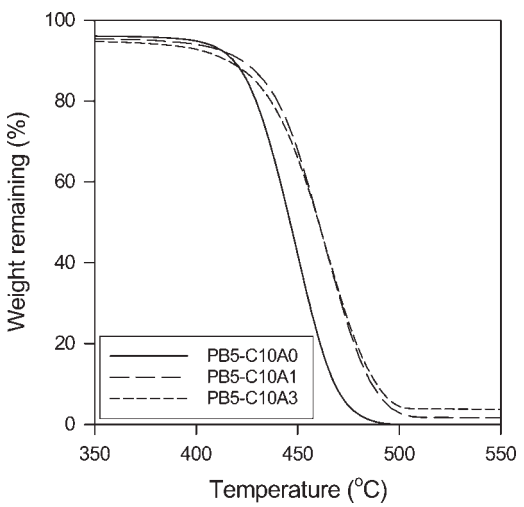

Figure 5 TGA thermograms of HIPS/organoclay nanocomposites.

TABLE IV
Average Molecular Weights of HIPS/Organoclay Nanocomposites

Sample code	M_w ($\times 10^5$)	M_n ($\times 10^5$)	PDI
PB3–C10A1	369	118	3.13
PB5–C10A0	421	125	3.37
PB5–C10A1	364	120	3.03
PB5–C10A3	337	109	3.09
PB8–C10A1	354	129	2.74

M_n = number-average molecular weight (g/mol); M_w = weight-average molecular weight (g/mol); PDI polydispersity index (M_w/M_n).

Attractive interactions between silicate layers and host polymers can significantly change the rheological behavior of polymer/organoclay nanocomposites in the molten state, depending on the aspect ratio and dispersion of clay incorporated.[2,24,25] In this study, rheological properties were measured to investigate the effect of the organoclay content on the flow behavior. As shown in Figure 6, the storage modulus and the complex viscosity gradually increased as the organoclay content increased. In the dispersions of organoclay in polymer melts, the rheological properties of these dispersions are believed to be rich and intimately linked to the

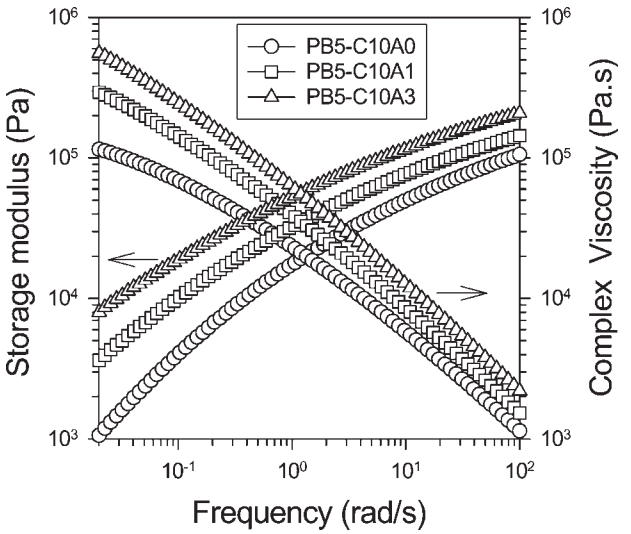

Figure 6 Storage modulus and complex viscosity of HIPS/organoclay nanocomposites.

mesoscopic structure of the inorganic filler in the dispersions. With the addition of only 1% organoclay, the storage modulus increased in a low frequency range, and the slope became less steep; this indicated the formation of a network-like structure due to a greater interaction between the polymer chains and silicate layers. The rheological data for the sample prepared by the addition of 3% organoclay were slightly higher than the data obtained from the addition of 1% clay. Because this comparison is drawn from the different molecular weights of the polymer matrices, as shown in Table IV, the marginal increase in the rheological properties would be substantial if the comparison were made with nanocomposites composed of a PS matrix with the same molecular weight. When the content of the organoclay with a high aspect ratios increases, therefore, the rheological properties of HIPS/organoclay nanocomposites may change from a liquid-like state to a solid-like state or from melt-like structures to network-like structures. Here, the overall change in the flow behavior depends on the degree of dispersion of the silicate layers acting as inert fillers or physical crosslinkers.

Gas-barrier properties

The gas-barrier properties of materials are important, especially in packaging applications. Because silicate layers are considered impenetrable by gas molecules, their addition to polymer films will enhance the barrier properties by forcing the gas molecules to experience a more tortuous path presented by the high-aspect-ratio clay as they diffuse through the films. This has been observed for many polymer/layered silicate and polymer/fumed silica nanocomposites.[11,26,27] For the prepared HIPS/organoclay nanocomposites, the permeability of N_2, O_2, and CO_2 gases through composite films was measured, and they are summarized in Table V. The permeability decreased with increasing clay content, whereas it increased with the rubber content; this reflects that clay, PS, and PB are in the order of increasing gas permeability. For the gas species tested, the permeability of O_2 was greater than that of N_2 and lower than that of CO_2 in samples with the same clay and rubber contents. This behavior was attributed to the different sizes of the molecules of the gases. It is reported in the literature that the kinetic diameters of N_2, O_2, and CO_2 are 364, 346, and 330 pm, respectively, and of the three gases, CO_2 gas shows higher solubility with respect to polymer films.[28–30] Because the permeability is the product of the diffusion coefficient and the solubility parameter, CO_2 gas can more easily pass through HIPS/organoclay nanocomposite films. However, the selectivity between two different gases, which is a yardstick of the separation ability of mixed gases and is shown in Table V, was not notably different in the films tested in this study, regardless of the clay and rubber contents involved. The permeability of air can be simply estimated from the permeability

TABLE V
Gas Permeabilities and Selectivities of HIPS/Organoclay Nanocomposites

	Permeability [(cm^3 mm)/(m^2 day atm)]			Selectivity		
Film type	$P(N_2)$	$P(O_2)$	$P(CO_2)$	$P(CO_2)/P(N_2)$	$P(O_2)/P(N_2)$	$P(CO_2)/P(O_2)$
PB3–C10A0	36.35	281.73	1272.5	35.01	7.75	4.52
PB3–C10A1	38.01	275.33	1195.94	31.46	7.24	4.34
PB3–C10A3	23.82	183.18	857.92	36.01	7.69	4.68
PB5–C10A0	45.48	304.73	1432.80	31.50	6.70	4.70
PB5–C10A1	35.25	256.68	1221.81	34.66	7.28	4.76
PB5–C10A3	29.05	212.79	1009.61	34.75	7.32	4.74
PB8–C10A0	60.88	389.08	1923.09	31.59	6.39	4.94
PB8–C10A1	41.58	277.92	1273.25	30.62	6.68	4.58
PB8–C10A3	35.98	236.23	1203.53	33.45	6.57	5.09

values of N_2 and O_2, the two main components of air, and is presented in Figure 7 together with the data for N_2 and O_2. As the clay content increases, it seems that the permeability decreases rapidly for O_2 versus N_2 and for the film with a higher rubber content. To identify the key factor that influences the barrier properties as the amount of clay increases, the normalized permeability, which is defined as the permeability ratio of the HIPS/organoclay nanocomposite to the HIPS polymer without any clay, was calculated. Figure 8 shows that the enhancement of gas-barrier properties by the addition of clay was more significant with a higher rubber content but was not discernable for the types of gases tested in this study. Lastly, it should be noted that the average molecular weights of the polymer matrices were not the same for each HIPS/organoclay nanocomposite, as described earlier. The gas-barrier properties would improve with the clay content if the comparison were made with samples having the same molecular weight.

Mechanical properties

Tensile and impact tests were conducted to evaluate the end-use mechanical properties of the HIPS/organoclay nanocomposites. The tensile modulus, tensile strength, and elongation at break obtained from tensile tests are presented in Figure 9 as a function of the clay content for various rubber contents. As the rubber content increased, the elongation at break increased as expected, but the tensile modulus and strength decreased. With the incorporation of the clay, the tensile modulus notably increased in comparison with that of the clay-free HIPS, whereas the tensile strength slightly decreased and the elongation at break greatly decreased. However, we note

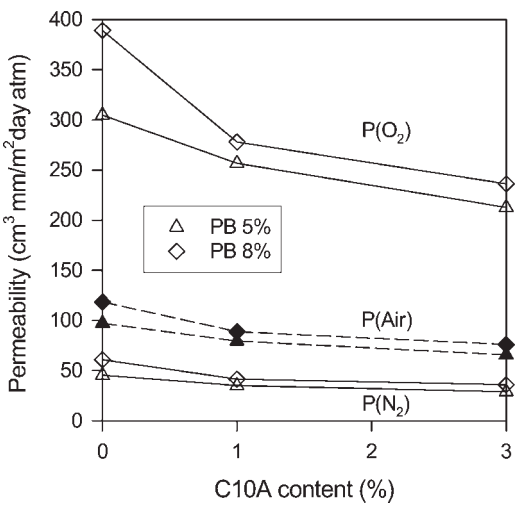

Figure 7 Nitrogen, oxygen, and air permeabilities of HIPS/organoclay nanocomposites.

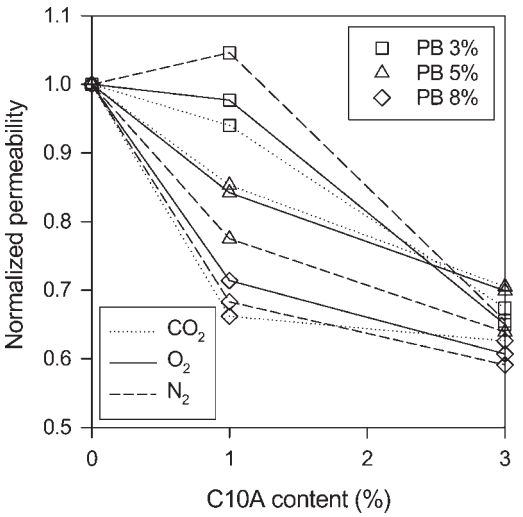

Figure 8 Normalized permeabilities of HIPS/organoclay nanocomposites.

that for the HIPS/organoclay prepared by *in situ* polymerization in this study, the improvement in the tensile modulus was higher and the reduction in the elongation at break was lower than those of the HIPS/organoclay nanocomposites prepared by the melt-intercalation method.[31] Because the average molecular weight of a polymer matrix prepared with a higher clay content is smaller than that of a polymer matrix prepared with a lower one, the actual effect of the incorporation of clay would be far better than the results obtained so far. The impact strength obtained from an impact test is plotted in Figure 10. As expected, the impact strength decreased with the introduction of stiff and inorganic materials. The main reason for the reduction of the impact strength is believed to be the silicate portion existing inside the rubber domain. Thus, an alternative way of preparing the nanocomposites with a minimal loss of impact properties was considered. In the synthesis of HIPS nanocomposites via the Synthetic route B (SynB) procedure, the organoclay was added right after the formation of the rubber phase. The results for the nanocomposites via the new SynB procedure are shown as open symbols with dashed lines in Figures 9 and 10. The improvement of the impact strength shown here is quite promising. An in-depth analysis of the characterization and properties of HIPS/organoclay nanocomposites prepared with the new procedure is currently underway.

CONCLUSIONS

HIPS/organoclay nanocomposites were synthesized via *in situ* bulk polymerization, and their properties were investigated. Among the commercial organoclays tested in this study, C10A, an organoclay with a benzyl unit similar to the structure of styrene, was

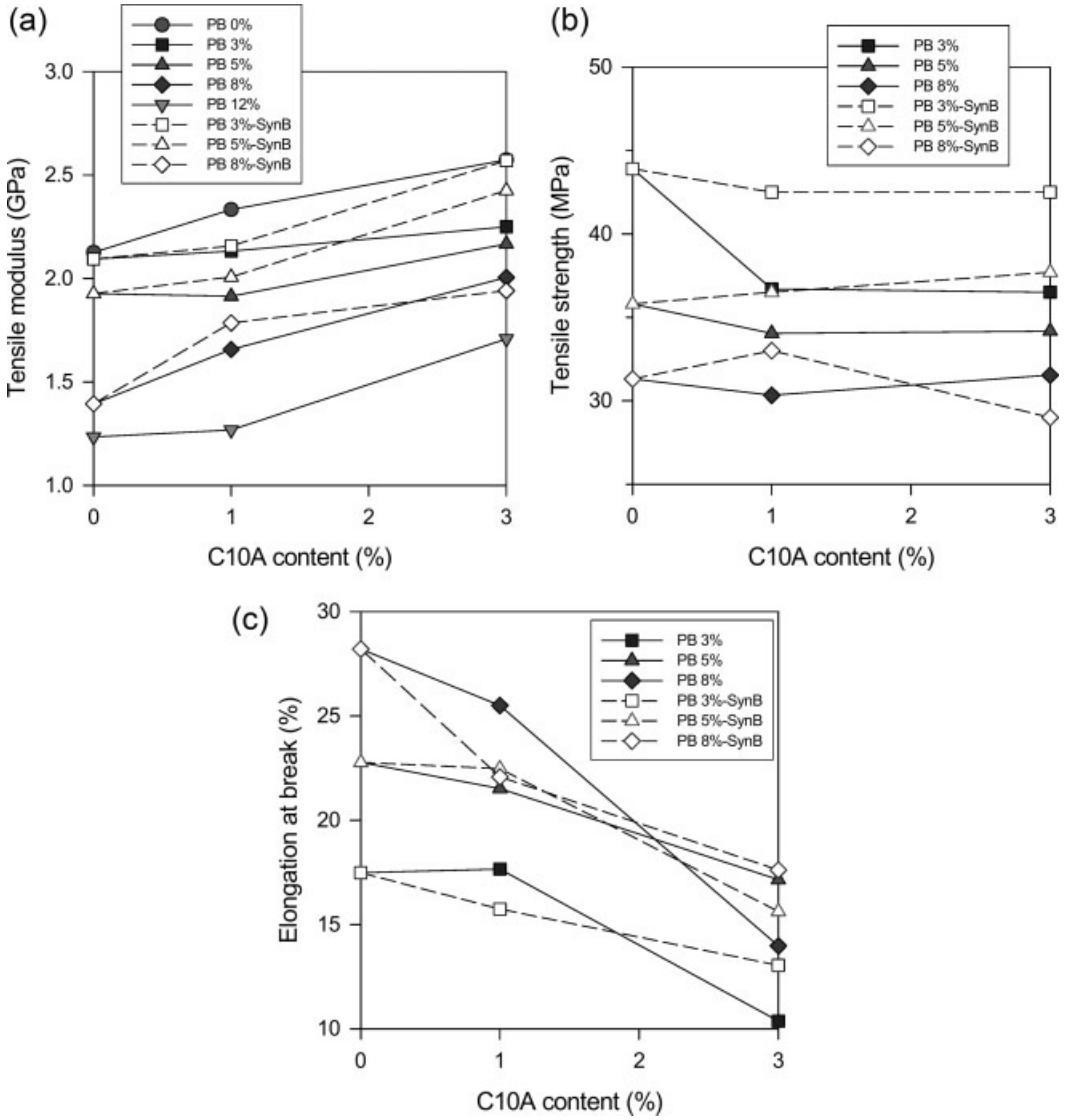

Figure 9 Tensile properties of HIPS/organoclay nanocomposites: (a) tensile modulus, (b) tensile strength, and (c) elongation at break.

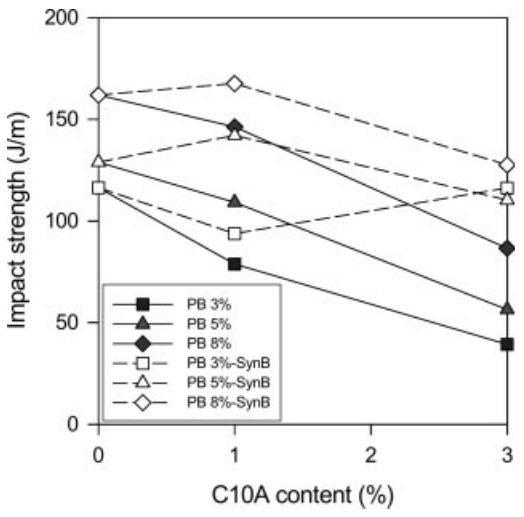

Figure 10 Impact strength of HIPS/organoclay nanocomposites.

most effective in achieving PS intercalation between silicate layers, as confirmed by XRD and TEM analyses. The nanocomposites showed intercalated structures in a global sense, but the silicate dispersions were different in the PS matrix phase and in the PB rubber phase because of the different affinities between the host material and clay. The average rubber domain size increased and its size distribution widened as the clay content increased, and this may have been caused by the unstable inversion and bridging effects due to the existence of silicate. The thermal stability and viscosity increased with the organoclay content, and they may have been influenced by a competition between the incorporation of clay and the decrease in the molecular weight of the polymer matrix. The gas-barrier properties increased with the clay content and decreased with the rubber content. The tensile modulus increased but the

impact strength decreased as the organoclay content increased. Nanocomposites with a minimal loss of impact strength could be prepared by changes in the synthetic procedure.

References

1. Giannelis, E. P. Adv Mater 1996, 8, 29.
2. Hoffmann, B.; Dietrich, C.; Thomann, R.; Friedrich, C.; Mulhaupt, R. Macromol Rapid Commun 2000, 21, 57.
3. Kojima, Y.; Usuki, A.; Kawasumi, M.; Okada, A.; Fukushima, Y.; Kurauchi, T.; Kamigaito, O. J Mater Res 1993, 6, 1185.
4. Akelah, A.; Moet, A. J Mater Sci 1996, 31, 3589.
5. Doh, J. G.; Cho, I. Polym Bull 1998, 41, 511.
6. Weimer, M. W.; Chen, H.; Giannelis, E. P.; Sogah, D. Y. J Am Chem Soc 1999, 121, 1615.
7. Zhu, J.; Wilkie, C. A. Polym Int 2000, 49, 1158.
8. Fu, X.; Qutubuddin, S. Polymer 2001, 42, 807.
9. Uthirakumar, P.; Song, M. K.; Nah, C.; Lee, Y. S. Eur Polym J 2005, 41, 211.
10. Uthirakumar, P.; Hahn, Y. B.; Nahm, K. S.; Lee, Y. S. Eur Polym J 2005, 41, 1582.
11. Yano, K.; Usuki, A.; Okada, A. J Polym Sci Part A: Polym Chem 1997, 35, 2289.
12. Alexandre, M.; Dubois, P. Mater Sci Eng 2000, 28, 1.
13. Giannelis, E. P.; Krishnamoorti, R.; Manias, E. Adv Polym Sci 1999, 118, 108.
14. Kojima, Y.; Usuki, A.; Kawasumi, M.; Okada, A.; Kurauchi, T.; Kamigaito, O. J Polym Sci Part A: Polym Chem 1993, 31, 1755.
15. Hwu, J. M.; Ko, T. H.; Yang, W. T.; Lin, J. C.; Jiang, G. J.; Xie, W.; Pan, W. P. J Appl Polym Sci 2004, 91, 101.
16. Zhu, L.; Wool, R. P. Polymer 2006, 47, 8106.
17. Oriakhi, C. Chem Br 1998, 34, 59.
18. Lee, S. J.; Jeoung, H. G.; Ahn, K. H. J Appl Polym Sci 2003, 89, 3672.
19. Stern, S. A.; Gareis, P. J.; Sinclair, T. F.; Mohr, P. H. J Appl Polym Sci 1963, 7, 2035.
20. Riess, G.; Gaillard, P. In Polymer Reaction Engineering; Reichert, K. H.; Geiseler, W., Eds.; Hanser: New York, 1983.
21. Jeoung, H. G.; Chung, D.; Ahn, K. H.; Lee, S. J.; Lee, S. J. Polymer (Korea) 2001, 25, 744.
22. Lee, S. J.; Chun, B. C.; Ahn, K. H.; Lee, S. J. J Chem Eng Jpn 2004, 37, 2.
23. Balazs, A. C.; Singh, C.; Zhulina, E.; Lyatskaya, Y. Acc Chem Res 1999, 8, 651.
24. Gelfer, M. Y.; Song, H. H.; Liu, L.; Hsiao, B. S.; Chu, B.; Rafailovich, M.; Si, M.; Zaitsev, V. J Polym Sci Part B: Polym Phys 2003, 41, 44.
25. Krishnamoorti, R.; Giannelis, E. P. Macromolecules 1997, 30, 4097.
26. Ray, S.; Yamada, K.; Okamoto, M.; Ogami, A.; Ueda, K. Chem Mater 2003, 15, 1456.
27. Vladimirov, V.; Betchev, C.; Vassiliou, A.; Papageorgiou, G.; Bikiaris, D. Compos Sci Technol 2006, 66, 2935.
28. Freeman, B. D. Macromolecules 1999, 32, 375.
29. Breck, D. W. Zeolite Molecular Sieves; Wiley: New York, 1974.
30. Suer, M. G.; Bac, N.; Yilmaz, L. J Membr Sci 1994, 91, 77.
31. Zhang, J.; Jing, D. D.; Wang, D.; Wilkie, C. A. Polym Degrad Stab 2006, 91, 2665.